ADVANCED FUNCTIONAL MATERIALS
www.afm-journal.de

Materials Views
www.MaterialsViews.com

Conformal Nano-Sized Inorganic Coatings on Mesoporous TiO_2 Films for Low-Temperature Dye-Sensitized Solar Cell Fabrication

By *Larissa Grinis, Sveta Kotlyar, Sven Rühle, Judith Grinblat,* and *Arie Zaban**

Here, a new method based on sol–gel electrophoretic deposition to produce uniform high-quality inorganic conformal coatings on mesoporous nanoparticulate films is presented. This novel sol preparation method allows for very fine control of the coating properties, thus inducing new adjustable functionalities to these electrodes. It is shown that the deposition of an amorphous TiO_2 and/or MgO shell onto photoanodes used in dye-sensitized solar cells (DSSCs) improves their light-to-electric-power conversion efficiency without the need for sintering. It is proposed that the amorphous TiO_2 coating improves the electronic inter-particle connection and passivates the surface states. The insulating MgO coating further reduces the electron transfer from the conduction band into the electrolyte while the electron injection from the excited dye state remains unperturbed for thin coatings. Using a low-temperature method for DSSC production on plastic substrates, a maximum efficiency of 6.2% applying pressure together with an optimized TiO_2 coating is achieved. For systems that cannot be pressed a conversion efficiency of 5.1% is achieved using a double shell TiO_2/MgO coating.

1. Introduction

Direct conversion of sunlight into electric power by solar cells is a sustainable and environmentally friendly energy resource. Dye-sensitized solar cells (DSSCs) have attracted substantial interest as a low-cost alternative to conventional silicon-based solar cells. They consist of a nanocrystalline, mesoporous, wide-bandgap semiconductor (usually TiO_2) that is covered with a monolayer of dye molecules and deposited onto a transparent conductive oxide (TCO). Upon illumination, electrons are injected from the photo-excited dye into the semiconductor while the pores are filled with a redox mediator, which reduces the oxidized dye and transports the positive charge to a counter electrode. Electrons diffuse through tens to hundreds of particles before they reach the TCO substrate, emphasizing the importance of good electronic inter-particle connection. Furthermore, recombination plays a critical role because of the extremely large TiO_2/dye/electrolyte interface area and the proximity of electrons to the oxidized redox species (the hole carriers), which can limit the photovoltaic performance.[1]

DSSCs have the potential to be produced on flexible plastic substrates, and are compatible with a roll-to-roll process to reduce fabrication costs. Flexible DSSCs are lightweight and thus very suitable to provide electric power to small and medium-size off-grid applications such as cellular phones or car batteries. On rigid glass substrates light-to-electric-power conversion efficiencies of up to 11% have been reported,[2] however, sintering at 450–550 °C is required to establish good electrical connections between the nanocrystals. This creates a major obstacle for plastic substrates that can only sustain temperatures up to about 150 °C. Common post-treatments to improve the connectivity between the nanocrystals, such as electrode treatment with $TiCl_4$ solution,[3] the anodic oxidative hydrolysis of $TiCl_3$,[4] or the cathodic electrodeposition of a titanium oxyhydroxide gel film with occluded TiO_2 (P-25) nanoparticles,[5] improve the cell performance but usually also require additional sintering. The same applies to using coatings that reduce recombination, such as Nb_2O_5,[6,7] Al_2O_3,[8,9] and $CaCO_3$.[10] A tedious method to transfer a sintered mesoporous TiO_2 film onto a plastic substrate has also been proposed, but this process was neither low cost nor suitable for up-scaling.[11]

Low-temperature methods based on hydrothermal crystallization,[12] UV exposure,[13] and chemical vapor deposition of Ti^{IV} alkoxides at 80 °C followed by exposure to UV light[14] have been presented, as well as coatings consisting of Mg, Zn, Al, or La hydroxides, which enhanced the performance of a non-sintered cell up to 4.7%.[15] Solar cells based on mesoporous SnO_2 films were improved by ZnO, TiO_2, or MgO shells.[16–18] DSSCs based on high surface area ITO electrodes showed reasonable efficiencies when coated with an amorphous TiO_2 or a double-shell TiO_2/MgO layer, whereas without such coatings they were not active at all.[19] It was also shown that low-temperature deposited amorphous TiO_2 coatings greatly enhanced the photostability of quantum-dot-sensitized solar cells.[20] Recently, plastic DSSCs with conversion efficiencies of up to 7.4% have been reported for small cell areas ($\leq$0.25 cm^2),[21] but a considerable error needs to be added to the efficiency value because of the small cell area.

We have developed a new low-temperature method to produce conformal coatings on non-sintered preformed mesoporous

[*] Prof. A. Zaban, Dr. L. Grinis, S. Kotlyar, Dr. S. Rühle, Dr. J. Grinblat
Institute of Nanotechnology & Advanced Materials
Bar Ilan University
Ramat Gan 52900 (Israel)
E-mail: zabana@mail.biu.ac.il

DOI: 10.1002/adfm.200901717

electrodes using a combination of sol–gel processing and electrophoretic deposition (EPD) to improve the electronic connection between the nanocrystals and to suppress recombination. This new method opens a path for the fabrication of efficient DSSCs based on plastic substrates using processes that do not involve temperatures exceeding 150 °C. Thin, amorphous coatings of TiO_2, MgO, and Nb_2O_5 were deposited onto mesoporous TiO_2 electrodes with the ability to control the thickness in the sub-nanometer regime. High-resolution transmission electron microscopy (HRTEM) images show that the coatings are conformal, uniform, continuous, and dense. We applied TiO_2, MgO, and TiO_2/MgO bilayer coatings to non-sintered electrodes. Using this mild coating method we succeeded to improve the conversion efficiency of non-sintered electrodes up to 6.2%.

2. Results

Low-temperature fabrication of DSSCs requires a method to electronically connect the individual nanoparticles and to create a barrier on the nanoparticle surface to suppress recombination. These properties can be achieved by a conformal coating of the nanoporous electrode surface. However, to attain a high performance fine control of the coating thickness and uniformity is needed. Our approach of controlled coating involves EPD of inorganic/organic metal oxo-polymers created by hydrolysis and condensation of metal alkoxides in alcohol solutions by adding iodine, acetone, and water. With this new method very stable sols are obtained with charged colloidal clusters that can be used for EPD with a fine control of the thickness of the conformal coating. Electrophoretic deposition of metal oxide layers requires the following: a) The sol has to be stable, containing only small colloidal clusters/particles. b) The colloidal clusters have to be electrically charged and the sol should have a low ionic strength to permit EPD. c) The presence of organic groups in colloidal clusters should be minimized to avoid contamination of the inorganic layer. d) Auxiliary materials applied during sol preparation should be easy to remove at low temperature (<150 °C).

Sol–gel processes based on metal alkoxides are well established,[22–25] however, sols fulfilling all the requirements above have so far not been developed. Typically, metal alkoxides (metal oxide precursors) are very sensitive to moisture.[25] Their hydrolysis is followed by condensation reactions leading to the formation of metal oxide particles and hydroxide clusters with some amount of attached organic groups because of incomplete hydrolysis. To obtain transparent sols control of the hydrolysis and condensation is necessary, which can be achieved through the use of inhibitors such as inorganic acids or complexing ligands, such as glycols, organic acids, and β-diketones.[22,24,25] Organic complexing ligands require high temperatures to remove them from the final deposit, and inorganic acids such as hydrochloric acid or nitric acid have to be applied in quite high concentrations which is detrimental to the EPD process.

Our deposition process is based on alcohol solutions containing iodine, acetone, and water, which lead to the formation of free H^+ ions by the following reactions:[26]

$$\begin{aligned} &CH_3COH_3 \leftrightarrow CH_3C(OH)CH_2 \\ &CH_3C(OH)CH_2 + I_2 \rightarrow CH_3COCH_2I + H^+ + I^- \end{aligned} \quad (1)$$

The first reaction is a keto–enol equilibrium catalyzed by water and iodine, followed by the second reaction between the enol-acetone and iodine resulting in H^+ ions. It is well known that protons are the simplest inhibitors for condensation reactions.[24] At the same time the protons adsorb on the surface of the colloidal metal oxide clusters, and the surface charge stabilizes the sol and enables EPD. The sol–gel EPD process was carried out from dilute solutions at low current densities (25–100 μA cm^{-2}). Under such conditions particles deposit slowly and individually, forming a tightly and uniformly packed layer.[27] Moreover, the use of EPD to attract the charged clusters ensures a conformal coating, even on mesoporous electrodes, with excellent thickness control defined by the sol concentration, deposition time, and current density. After deposition all auxiliary components of the sols such as iodine, acetone, water, and low alcohols can be removed at low temperature. The sol is very stable and can be stored for months. This method is very simple and reproducible; coatings can be prepared over a short time and with simple equipment. Although traces of organic groups can be present in the resulting coatings (shells) because

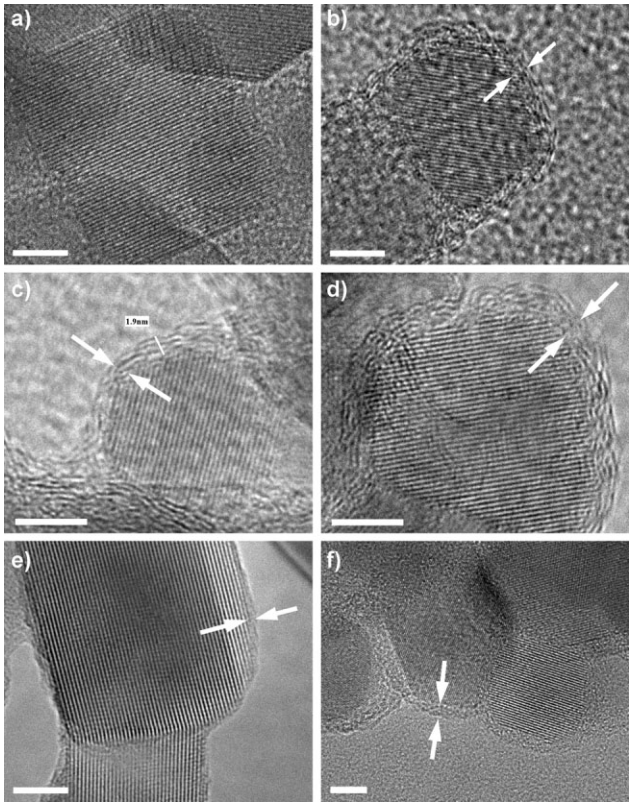

Figure 1. High-resolution TEM images of a) uncoated TiO_2 nanoparticles (P25) showing the crystalline particle surface. b) TiO_2 nanoparticles homogeneously coated with a conformal amorphous titania shell before any heat treatment. c) Heating the coated TiO_2 samples at 150 °C for 4 h does not change the morphology of the titania coating. d) TiO_2 nanoparticles coated with titania after sintering at 500 °C for 60 min. e) TiO_2 nanoparticles coated with a thin magnesia shell after drying at 150 °C for 4 h. f) TiO_2 nanocrystals coated with an amorphous niobia layer. The scale bar in each image represents a length of 5 nm and white arrows indicate the coating thickness.

of incomplete hydrolysis of the precursors, for simplicity reasons the coatings below will be named ''titania'', ''magnesia'' and ''niobia''.

Figure 1a shows a high-resolution transmission electron microscopy (HRTEM) image of TiO_2 (P-25) nanoparticles without coating where the surface facets of the nano-crystals are clearly visible. TiO_2 particles coated with titania by sol–gel EPD without further thermal treatment are presented in Figure 1b. It can be seen that the coating is amorphous and forms a very uniform, homogeneous, compact, and continuous conformal shell on the mesoporous film surface. The shell thickness could be varied from a few Ångstroms to a few nanometers depending on the sol concentration, current density, and deposition time. Figure 1c shows the same amorphous TiO_2 coating as in Figure 1b, but after drying at 150 °C for 4 h. It is clear that such thermal treatment did not lead to crystallization and had a negligible effect on the shell thickness, uniformity, homogeneity, compactness, and continuity of the coating. The coating remained amorphous up to 400 °C after which crystallization may occur, which is not directly visible from the HRTEM image (Fig. 1d) but was supported by X-ray diffraction and differential scanning calorimetry measurements (see Supporting Information). Even after sintering at 500 °C, when the coating thickness was less than 2–3 nm, the coating shell remained uniform, conformal, and continuous, whereas pinholes sometimes formed in thicker layers. Figure 1e shows a very thin (about 0.5 nm) conformal magnesia coating on TiO_2 P-25 nanoparticles, whereas Figure 1f shows a niobia coating on similar particles. The thickness of these shells could also be varied from a few Ångstroms to a few nanometers by increasing the sol concentration, current density, and deposition time, or by applying multiple deposition cycles. In all cases we achieved high-quality coatings, however, since low-temperature niobia coating did not improve the solar-cell performance it will not be discussed further.

Figure 2 illustrates the influence of the titania coating on the performance of DSSCs based on mesoporous TiO_2 electrodes, prepared by EPD,[28] dried, and processed without further mechanical compression or sintering. A thin amorphous coating was electrophoretically deposited followed by electrode drying at 150 °C for 4 h and sensitizing with a dye. Figure 2a shows that the current density–voltage (J–V) characteristics are strongly improved for the titania-coated electrode (180 s deposition time, 25 μA cm^{-2}) with respect to an uncoated electrode. The correlation of the short-circuit current density (J_{sc}), the open-circuit voltage (V_{oc}), the fill factor, and subsequently the light-to-electric-power conversion efficiency (η) as a function of the deposition time of the amorphous titania coating is shown in Figure 2b and c. The largest improvement in the J_{sc} (Fig. 2b) was observed after 3 min deposition. The fill factor (Fig. 2c) was higher for all coated electrodes with respect to the uncoated reference, whereby a rapid increase can be seen for short deposition times after which the fill factor remained almost constant for longer deposition times. The V_{oc} also improved for all coated electrodes being highest at short deposition times after which it decreased slightly with increasing coating thickness. Consequently, the amorphous TiO_2 coating increased the efficiency of the cells containing non-pressed non-sintered electrodes by up to 65% compared to the non-coated reference. The initial efficiency increase can be attributed to an improved electronic connection of the individual TiO_2 nanocrystals and reduced recombination rate. Furthermore, parts of the fluorine-doped tin oxide (FTO) substrate that are in contact with the electrolyte are also coated, thus decreasing recombination from the FTO into the electrolyte. Increasing the deposition duration beyond 10 min resulted in a sharp fall of all solar cell parameters (not shown) as thick coatings reduce the injection efficiency and can hinder ion motion within the mesoporous structure.

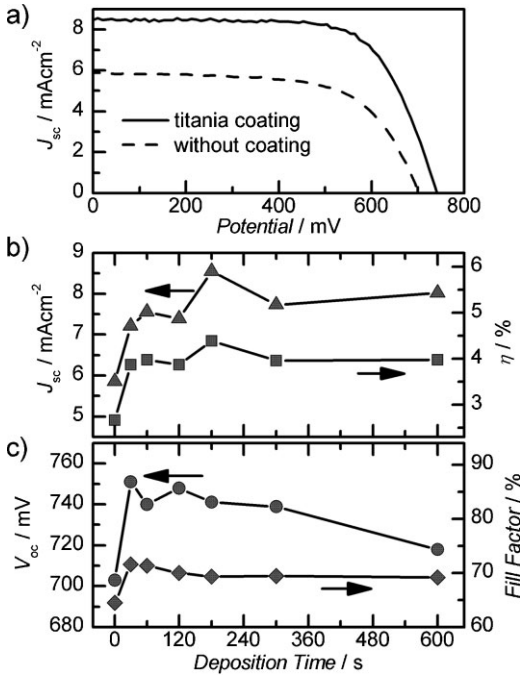

Figure 2. Amorphous TiO_2-coated non-pressed mesoporous electrodes (16–17 μm film thickness) after drying at 150 °C for 4 h without further sintering. a) The J–V characteristics of the amorphous TiO_2-coated electrode (solid) shows a strong improvement compared to an uncoated electrode. b) J_{sc} and η as a function of deposition time of the amorphous TiO_2 shell (deposition current density $J_{dep} = 25$ μA cm^{-2}). The parameters of the uncoated electrode are plotted at 0 s deposition time. c) V_{oc} and fill factor as a function of the coating time showing a strong increase after short coating times and smaller improvements after that for longer coating times.

Magnesia coating on non-pressed and non-sintered electrodes turned out to be detrimental for their photovoltaic performance (not shown). Unlike the titania shell, magnesia is insulating. It can penetrate in between poorly connected nanoparticles and form a dielectric barrier, which prohibits efficient electronic transport. This restriction can be lifted when the magnesia coating is applied to electrodes that are pre-coated with an amorphous TiO_2 shell. Figure 3a shows the J–V characteristics of a non-coated reference cell compared to a single-layer titania-coated electrode (3 min deposition time) and a titania/magnesia bi-layer coated electrode. A huge improvement of the solar cell parameters can be observed (Figs. 3b and c) after the deposition of the titania layer similar to that in Fig. 2 (small differences result from variations of the mesoporous film thickness). Subsequently, deposition of magnesia led to a further increase of the cell performance, and all cell parameters were improved. We propose that the titania coating improves the electronic connection of adjacent TiO_2 nanoparticles while slowing down the recombination processes. The insulating

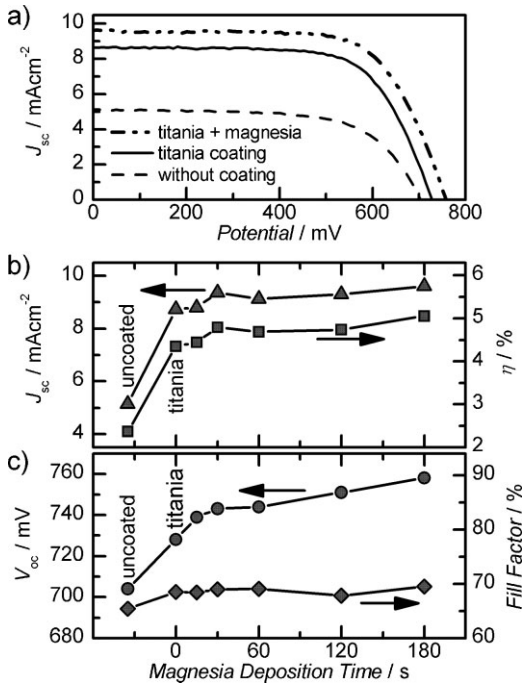

Figure 3. Non-pressed mesoporous TiO_2 electrodes (14–15 μm film thickness) coated with a magnesia/titania bilayer, after drying at 150 °C for 4 h. a) The *J–V* characteristics are strongly improved after 3 min of titania coating ($J_{dep} = 25$ μA cm^{-2}) and show a further performance increase after additional magnesia coating for 3 min ($J_{dep} = 50$ μA cm^{-2}). b) J_{sc} and η as a function of the magnesia deposition after titania coating (3 min). c) V_{oc} and fill factor as a function of the magnesia shell deposition time.

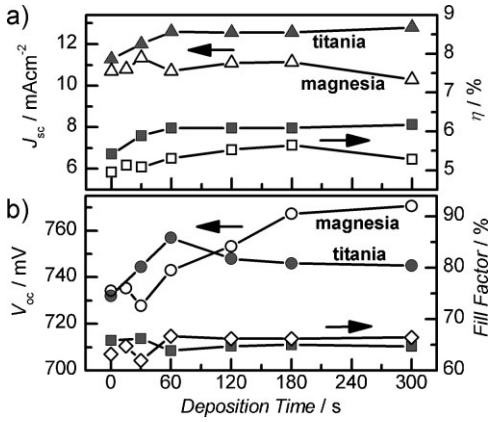

Figure 4. a) J_{sc} and η for pressed (1000 kg cm^{-2}) non-sintered electrodes, coated with a shell of titania (solid symbols) or magnesia (open symbols) as a function of the deposition time at $J_{dep} = 50$ μA cm^{-2}. The electrodes were dried at 150 °C for 4 h before they were sensitized with a dye. b) V_{oc} and fill factor as a function of the coating time.

magnesia coating improves the blocking properties of the shell, which was confirmed by open-circuit voltage decay analysis (see below) and dark *J–V* measurements (see Supporting Information). The conversion efficiency of non-pressed, non-sintered mesoporous TiO_2 electrodes was improved by 113% using the titania/magnesia bilayer coating.

To investigate the effect of a magnesia coating without a precoated titania shell alternative methods had to be employed to improve the electronic connection between the TiO_2 nanocrystals. Application of mechanical pressure is a low-temperature method suitable for plastic substrates, which can improve the electronic connection and adhesion of the mesoporous TiO_2 layer to a substrate. The effect of titania and magnesia coatings on pressed (1000 kg cm^{-2}) non-sintered electrodes is shown in Figure 4. The titania sol used for these experiments was diluted by a factor of 6.25 compared to the one used for non-pressed electrodes. Figure 4a and b show that the solar cell parameters of the pressed electrodes are significantly higher compared to those of the non-pressed samples (Fig. 2 and 3). Moreover, as for the non-pressed electrodes, a significant improvement in the conversion efficiency is observed for the titania-coated electrodes compared to the non-coated reference. The thin amorphous titania shell on the pressed electrodes improves mostly the J_{sc} whereas the V_{oc} shows only an initial increase at short coating times before it reaches a plateau. The fill factor remains practically constant. The best results for the amorphous titania-coated pressed electrode were achieved after a deposition time of 5 min where the conversion efficiency improved by 11% from 5.6% (non-coated) to 6.2%.

For the magnesia-coated pressed electrodes a higher efficiency is also observed compared to the non-coated electrode. We note that the magnesia solution used for coating was only half as concentrated as the titania solution used for the pressed coated electrodes, to enable us to relate tiny variations in the photovoltaic performance to the coating thickness. The best photocurrent and conversion efficiency were observed after 30 s and 1 min of deposition, respectively. After their maximum both parameters decreased with progressing deposition time. In contrast, the V_{oc} showed an increase up to 3 min deposition time before it reached a plateau whereas the fill factor changed very little. It has been shown before that magnesia forms a barrier layer at the TiO_2/electrolyte interface[1,6,7,9,17,18] and blocks electron transfer into the redox electrolyte, thus improving the V_{oc} of the device. The alkalinity of the magnesia surface is favorable for dye adsorption,[17] which can be the reason for the increased J_{sc} at short deposition times. However, an increasing coating thickness hinders electron transfer from the photo-excited dye state into the TiO_2. Using X-ray photoelectron spectroscopy (XPS) analysis an optimal magnesia shell thickness of several Ångstroms was estimated (see Supporting Information).

Open-circuit voltage decay (OCVD) analysis[8,29] was used to investigate in more detail the origin of the improved DSSC efficiency obtained with the titania and magnesia coatings. In the OCVD method, steady-state illumination at open circuit is switched off by a shutter and the V_{oc} is recorded as a function of time. It has been shown previously that OCVD analysis can provide information about the electron lifetime τ_e in nanoporous films.[29] At low voltage τ_e is determined by electron transfer from surface states at the quasi Fermi level into the electrolyte, while at higher voltages direct transfer from the conduction band states dominates.

Figure 5a represents the electron lifetime as a function of the open-circuit potential derived from OCVD data non-pressed electrodes coated with a single titania shell and for the titania/

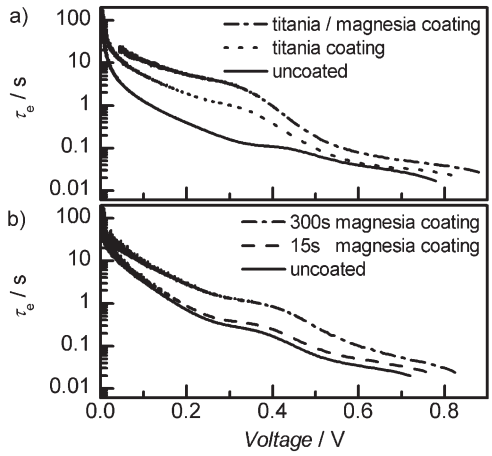

Figure 5. Electron lifetime τ_e, as a function of the applied potential derived from OCVD decay measurements: a) For non-pressed, non-sintered electrodes without coating (solid line), with titania coating (dotted line), and for bilayer coated titania/magnesia electrodes (dashed-dotted line). b) For pressed, non-sintered electrodes without coating (solid line), with a thin magnesia (dashed line), and a thick magnesia coating (dashed-dotted line).

magnesia bilayer-coated electrodes in comparison with a non-coated reference (same electrodes as in Fig. 3). The uncoated reference sample showed a lower electron lifetime at all potentials while the titania shell led to a substantial lifetime increase of almost one order of magnitude in the low-voltage regime (<0.4 V). At higher voltages τ_e approached the value of non-coated electrodes and is almost the same at potentials above 0.6 V. Double-shell-coated titania/magnesia electrodes showed an increase of the electron lifetime throughout the entire voltage range compared to both the titania-coated and uncoated electrodes. The advantage of the magnesia coating is the observed lifetime increase at voltages close to V_{oc}.

Figure 5b displays the effect of the magnesia shell on pressed, non-sintered mesoporous TiO_2 electrodes (identical to the ones shown in Fig. 4). We observed a slightly improved electron lifetime for a very thin magnesia shell (15 s deposition time) while the electron lifetime for a thicker shell (300 s deposition time) was approximately half an order of magnitude over the entire potential range. The pronounced lifetime improvement at high potentials is consistent with the enhanced V_{oc} which was observed from J–V measurements (Fig. 4).

In the low-voltage region the charge transfer is dominated by the surface states in the bandgap of TiO_2 nanocrystals. The improvement of τ_e in this regime after titania coating indicates that the amorphous shell mainly passivates the surface states. Previously reported photocurrent transient measurements also indicated that the coating passivates the surface states and improves inter-particle connection.[30] The magnesia shell increased the electron lifetime at medium and high voltages where the charge transfer is dominated by conduction band states.[29] We propose that the magnesia shell mainly reduces the rate of interfacial charge transfer from conduction band states into the electrolyte.

3. Discussion

The effect of titania and magnesia coating on the DSSC performance for non-pressed electrodes is schematically summarized in Figure 6 showing weakly connected nanocrystals (Fig. 6a and b) leading to a poor electron transport through the film. The homogenous conformal titania coating drastically increases the interface area between neighboring particles, and, probably, "glues" these particles together (Fig. 6c), which improves the electron transport (schematically shown by larger arrows) and, subsequently, the conversion efficiency. Coating with an insulating magnesia shell only creates an additional dielectric barrier at the neck in between particles hindering electron transport and decreasing the DSSC performance (Fig. 6d). The highest efficiency improvement on non-pressed electrodes was achieved with bilayer coatings (Fig. 6e). Here, the titania coating enhances the inter-particle connections, whereas the insulating magnesia layer creates a spatial and energetic barrier at the mesoporous TiO_2/dye/electrolyte interface, which suppresses electron recombination (shown by crossed-out arrows). The magnesia shell should be sufficiently thin though to allow electron transfer from the excited dye state into the TiO_2 by tunneling.

A DSSC based on a pressed mesoporous TiO_2 film is schematically depicted in Figure 7a. Mechanical pressure decreases the inter-particle distance and the porosity leading to improved electronic connection between the nanoparticles and, subsequently, to a better electron transport, compared to non-

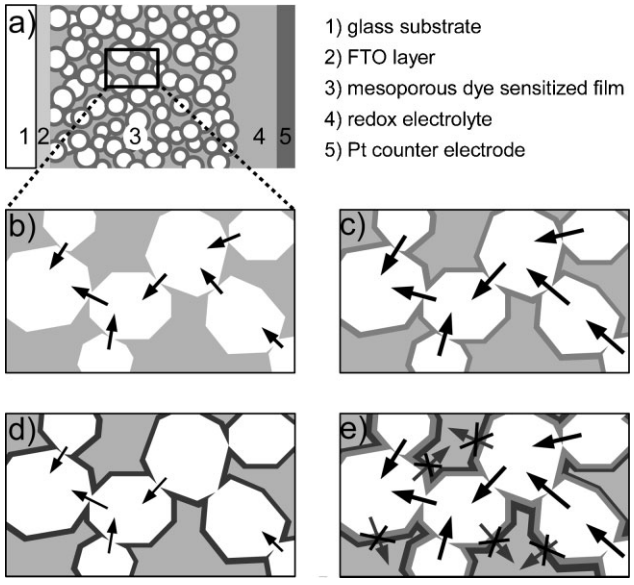

Figure 6. a) Schematic drawing of a DSSC based on a non-pressed TiO_2 film. b) TiO_2 nanocrystals in non-pressed films showing weak inter-particle connections. The dye-monolayer is not shown for simplicity. c) The titania coating (light gray) improves the inter-particle connections and, thus, electron transport through the mesoporous network and slows down the recombination processes. d) An insulating magnesia shell (dark gray) introduces a dielectric barrier in between the weakly connected particles and decreases the DSSC performance. e) A bilayer coating increases the DSSC efficiency because of improved inter-particle connection by the titania shell and an effective magnesia blocking layer that suppresses electron recombination into the electrolyte.

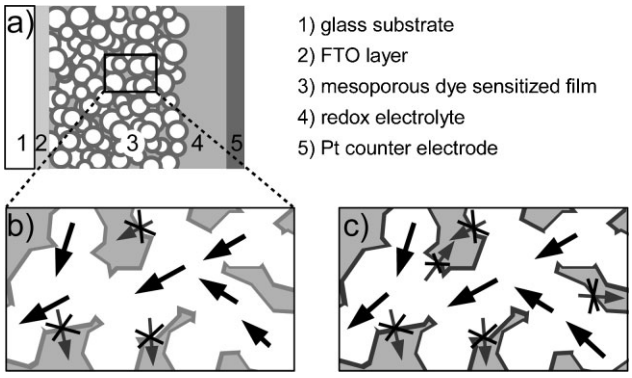

Figure 7. a) Schematic drawing of a DSSC based on a mechanically pressed mesoporous TiO_2 film. b) Mechanical compression improves the inter-particle connection; in this case the titania coating improves the DSSC performance mainly by passivating the surface states. c) Direct magnesia coating onto well-interconnected TiO_2 particles in pressed films improves the solar cell performance because of suppressed recombination.

pressed electrodes. The titania coating slightly increases the interfacial area of adjacent nanoparticles (Fig. 7b), however, the enhancement in the solar cell efficiency is mainly related to the passivation of the surface states and a subsequent reduction of the recombination. This is, furthermore, confirmed by measurements using magnesia-coated pressed electrodes, which also improved the cell performance (Fig. 7c). Because of the improved inter-particle connection in pressed films the magnesia coating does not hinder electron transport but decreases electron recombination into the electrolyte, thus improving the conversion efficiency.

4. Conclusions

Amorphous inorganic coatings can give new functionalities to mesoporous films. We have shown that conformal, uniform, continuous, and dense coatings can be produced by sol–gel EPD with excellent thickness control. In DSSCs, titania coatings improve the electronic connection between the nanocrystals of mesoporous electrodes and slow down the recombination processes. Insulating magnesia coatings improve the blocking properties of the shell further reducing electron recombination with the electrolyte. Sintering is not required, which makes the coating technique applicable to DSSCs on plastic substrates. A light-to-electric-power conversion efficiency of 6.2% was achieved by both applying pressure and a titania coating to non-sintered mesoporous photoelectrodes used in DSSCs.

5. Experimental

Materials: Tetraisopropyl orthotitanate (Merck); niobium isopropoxide 10% w/v in isopropanol/hexane (50:50) (Alfa Aesar); magnesium ethoxide (98%), iodine (99.8%), and tert-butylpyridine (99%) (all from Aldrich); acetylacetone (≥99.5%) and methoxypropionitrile (Fluka); absolute ethanol anhydrous (Gadot) with maximum water content 0.1%; analytical grade acetone (Frutarom Ltd.); and HPLC grade acetonitrile (J. T. Baker) with water content 0.002% were all used as received without further purification. The dye cis-dithiocyanato bis(4,4′-dicarboxylic acid-2,2′-bipyridine) ruthenium(II) commonly termed N3 was purchased from Dyesol (Australia). TiO_2 nanopowder P-25 was purchased from Degussa AG (Germany).

Mesoporous TiO2 Film Preparation: Fluorine-doped tin oxide (FTO)-coated glass substrates (Pilkington, bought from Hartford Glass Co. Inc., USA) with a sheet resistance of 15 Ω/square were cleaned with ethanol and mild soap, after which they were thoroughly rinsed with deionized water(18.2 MΩ), and dried in a filtered air stream. Mesoporous titania electrodes were prepared from commercially available TiO_2 P-25 nanocrystalline powder by EPD from ethanol suspensions with acetylacetone, iodine, acetone, and water additives as reported elsewhere [28]. The P-25 concentration in suspension was 2.4 g L^{-1} and the EPD was conducted in constant current mode with a current density of 0.4 mA cm^{-2} at room temperature. After drying at 150 °C for 30 min some electrodes were mechanically pressed using a hydraulic press (Bivas Hydraulic Industries Ltd.). The thickness of the TiO_2 films was measured with a Surftest SV 500 profilometer (Mitutoyo Co.).

Coating: Iodine (0.04–0.2 g L^{-1}) and acetone (8–20 mL L^{-1}) were dissolved in 250 mL of ethanol. Using an inert atmosphere glove box, 0.003–0.04 M of metal alkoxide was placed in a bottle, hermetically sealed, and transferred outside the glove box, where under ambient conditions the ethanol solution was added to the metal alkoxide under vigorous stirring, after which the solution was cooled to 0–15 °C in an ice bath. If necessary, the solution was sonicated until the metal alkoxide was dissolved, then under vigorous stirring deionized water (4–10 mL L^{-1}) was added and the solution was stirred for 24 h resulting in a transparent sol (except magnesium alkoxide which was slightly turbid, and was purified by centrifugation at 4000 rpm for 3–5 min.). The color of the solution gradually changed from yellow to colorless. The sol was left to age in a closed vessel without stirring at ambient conditions for a few days (typically, 7–10 days), before it was used for sol–gel EPD. In a closed vessel under ambient conditions, this sol stayed transparent and stable for at least several months. A ''concentrated' titania sol, used for the coating of non-pressed P-25 mesoporous electrodes, was prepared from 0.01 M tetraisopropyl orthotitanate, 100 mg L^{-1} of iodine, 16 mL L^{-1} of acetone, and 8 mL L^{-1} of water in ethanol. A ''diluted'' titania sol, used for the coating of pressed P-25 mesoporous electrodes, was prepared from 1.6 mM of tetraisopropyl orthotitanate, 80 mg L^{-1} of iodine, 16 mL L^{-1} of acetone, and 8 mL L^{-1} of water in ethanol. The magnesia sol was prepared from 0.8 M of magnesium ethoxide, 60 mg L^{-1} of iodine, 16 mL L^{-1} of acetone, and 8 mL L^{-1} of water in ethanol. The niobia sol was prepared from 5 mM niobia isopropoxide, 120 mg L^{-1} of iodine, 16 mL L^{-1} of acetone, and 8 mL $L^{-1}$of water in ethanol.

The electrophoretic cell contained two electrodes placed vertically and immersed in a prepared sol. The P-25 mesoporous electrode on conductive glass served as the cathode and a FTO conductive glass was used as a counter electrode with a distance of 54 mm between them. For thicker shells (2–6 nm) used for HRTEM imaging, the distance between the electrodes was 18 mm. The sol–gel EPD process was performed at room temperature at a constant current (25–100 μA cm^{-2}), using a Keithley 2400 Source Meter. All series of the samples were repeated 3 times and reproducibility was in the range of ± 10%.

Characterization: High-resolution transmission electron microscopy (JEOL, JEM-2010 microscope) was used to determine the uniformity, conformity, and thickness of the coating. Small amounts of coated mesoporous films were scraped from the conductive glass, mixed with ethanol, sonicated while cooled in an ice bath, drop-cast onto a carbon-coated copper grid, and dried. X-ray photoelectron spectroscopy (XPS) (Kratos AXIS HS) was employed to estimate the thickness of the magnesia coating as described before [6].

Photoelectrochemical Measurements: Mesoporous TiO_2 electrodes were immersed at a temperature of 80–100 °C after sensitizing in a 0.3 mM N3-dye solution in ethanol for 48–60 h at room temperature. Sensitized electrodes were rinsed with ethanol and dried under a filtered air stream. A two-electrode sandwich cell with an effective area of 0.635 cm^2 was employed to measure the performance of DSSCs using a Pt-coated FTO

layered glass as a counter electrode. Teflon tape with a thickness of 50 μm was positioned as a spacer between the two electrodes. The composition of the electrolyte was 0.6 M 1,2-dimethyl-3-propylimidazolium iodide, 0.1 M LiI, 0.05 M I_2, 0.5 M tert-butylpyridine in 1:1 acetonitrile/methoxypropionitrile. Photocurrent–voltage characteristics were performed using an EcoChemie Potentiostat. A 300 W xenon arc lamp (Oriel) calibrated to approximately 100 mW cm^{-2} served as the light source. The conversion efficiencies were not corrected for reflection and absorption losses of the conductive glass. For the open-circuit voltage decay measurements, the illumination was turned off with a shutter and the open-circuit voltage was recorded with an Ecochemie potentiostat equipped with a short-interval sampling module. Typically, the measurement interval was 10–50 ms. For OCVD measurements the composition of the electrolyte was: 0.5 M NaI and 0.05 M I_2 in γ-butyrolactone.

Acknowledgements

The authors acknowledge the support from the European Union ''OrgaPVnet'' project. SR acknowledges financial support from the European Union within the FP7 framework (Marie Curie Intra-European Fellowship for Career Development). Supporting information is available online from Wiley InterScience or from the author.

Received: September 10, 2009
Published online: November 17, 2009

[1] B. A. Gregg, F. Pichot, S. Ferrere, C. L. Fields, *J. Phys. Chem. B* **2001**, *105*, 1422.
[2] a) M. Grätzel, *Prog. Photovoltaics* **2006**, *14*, 429. b) B. O'Regan, M. Grätzel, *Nature* **1991**, *353*, 737.
[3] a) M. K. Nazeeruddin, A. Kay, I. Rodicio, R. Humphry-Baker, E. Müller, P. Liska, N. Vlachopoulos, M. Grätzel, *J. Am. Chem. Soc.* **1993**, *115*, 6382. b) P. M. Sommeling, B. C. O'Regan, R. R. Haswell, H. J. P. Smit, N. J. Bakker, J. J. T. Smits, J. M. Kroon, J. A. M. van Roosmalen, *J. Phys. Chem. B* **2006**, *110*, 19191.
[4] L. Kavan, B. O'Regan, A. Kay, M. Grätzel, *J. Electroanal. Chem.* **1993**, *346*, 291.
[5] J. Yamamoto, A. Tan, R. Shiratsuchi, S. Hayase, C. R. Chenthamarakshan, K. Rajeshwar, *Adv. Mater.* **2003**, *15*, 1823.
[6] S. G. Chen, S. Chappel, Y. Diamant, A. Zaban, *Chem. Mater.* **2001**, *13*, 4629.
[7] A. Zaban, S. G. Chen, S. Chappel, B. A. Gregg, *Chem. Commun.* **2000**, 2231.
[8] F. Fabregat-Santiago, J. Garcia-Canadas, E. Palomares, J. N. Clifford, S. A. Haque, J. R. Durrant, G. Garcia-Belmonte, J. Bisquert, *J. Appl. Phys.* **2004**, *96*, 6903.
[9] E. Palomares, J. N. Clifford, S. A. Haque, T. Lutz, J. R. Durrant, *J. Am. Chem. Soc.* **2003**, *125*, 475.
[10] a) N. Okada, S. Karuppuchamy, M. Kurihara, *Chem. Lett.* **2005**, *34*, 16. b) Z.-S. Wang, M. Yanagida, K. Sayama, H. Sugihara, *Chem. Mater.* **2006**, *18*, 2912.
[11] M. Dürr, A. Schmid, M. Obermaier, S. Rosselli, A. Yasuda, G. Nelles, *Nat. Mater.* **2005**, *4607*.
[12] a) D. Zhang, T. Yoshida, H. Minoura, *Adv. Mater.* **2003**, *15*, 814. b) D. Zhang, T. Yoshida, K. Furuta, H. Minoura, *J. Photochem. Photobiol. A* **2004**, *164*, 159.
[13] Z. Tebby, O. Babot, D. Michau, L. Hirsch, L. Carlos, T. Toupance, *J. Photochem. Photobiol. A* **2009**, *205*, 70.
[14] T. Miyasaka, Y. Kijitori, T. N. Murakami, M. Kimura, S. Uegusa, *Chem. Lett.* **2002**, *31*, 1250.
[15] J.-H. Yum, S. Nakade, D.-Y. Kim, S. Yanagida, *J. Phys. Chem. B* **2006**, *110*, 3215.
[16] S. Chappel, S.-G. Chen, A. Zaban, *Langmuir* **2002**, *18*, 3336.
[17] A. Kay, M. Grätzel, *Chem. Mater.* **2002**, *14*, 2930.
[18] K. Tennakone, P. K. M. Bandaranayake, P. V. V. Jayaweera, A. Konno, G. R. R. A. Kumara, *Phys. E* **2002**, *14*, 190.
[19] L. Grinis, A. Ofir, S. Dor, S. Yahav, A. Zaban, *Isr. J. Chem.* **2008**, *48*, 269.
[20] M. Shalom, S. Dor, S. Rühle, L. Grinis, A. Zaban, *J. Phys. Chem. C* **2009**, *113*, 3895.
[21] a) T. Miyasaka, M. Ikegami, Y. Kijitori, *J. Electrochem. Soc.* **2007**, *154*, A455. b) K.-M. Lee, S.-J. Wu, C.-Y. Chen, C.-G. Wu, M. Ikegami, K. Miyoshi, T. Miyasaka, K.-C. Ho, *J. Mater. Chem.* **2009**, *19*, 5009. c) T. Yamaguchi, N. Tobe, D. Matsumoto, H. Arakawa, *Chem. Commun.* **2007**, 4767.
[22] a) D. D. Dunuwila, C. D. Gagliardi, K. A. Berglund, *Chem. Mater.* **1994**, *6*, 1556. b) B. E. Yoldas, *J. Mater. Sci.* **1986**, *21*(3), 1087.
[23] J. H. Jean, T. A. Ring, *Langmuir* **1986**, *2*(2), 251.
[24] a) J. Blanchard, S. Barboux-Doeuff, J. Maquet, C. Sanchez, *New J. Chem.* **1995**, *19*, 929. b) M. Kallala, C. Sanchez, B. Cabane, *Phys. Rev. E* **1993**, *48*, 3692.
[25] a) J. Livage, M. Henry, C. Sanchez, *Prog. Solid State Chem.* **1988**, *18*, 259. b) C. Sanchez, F. Ribot, *New J. Chem.* **1994**, *18*, 1007.
[26] N. Koura, T. Tsukamoto, H. Shoji, T. Hotta, *Jpn. J. Appl. Phys.* **1995**, *34*, 1643.
[27] a) P. Sarkar, P. S. Nicholson, *J. Am. Ceram. Soc.* **1996**, *79*, 1987. b) I. Zhitomirsky, *Adv. Colloid Interface Sci.* **2002**, *97*, 277.
[28] a) L. Grinis, S. Dor, A. Ofir, A. Zaban, *J. Photochem. Photobiol. A* **2008**, *198*, 52. b) S. Dor, S. Rühle, A. Ofir, M. Adler, L. Grinis, A. Zaban, *Colloids Surf. A* **2009**, *342*, 70.
[29] a) J. Bisquert, A. Zaban, M. Greenshtein, I. Mora-Sero, *J. Am. Chem. Soc.* **2004**, *126*, 13550. b) A. Zaban, M. Greenshtein, J. Bisquert, *ChemPhysChem* **2003**, *4*, 859.
[30] A. Ofir, T. Dittrich, S. Tirosh, L. Grinis, A. Zaban, *J. Appl. Phys.* **2006**, *10*, 074317.